Development of traffic induced permanent strain in concrete block pavements

M. Huurman
Laboratory for Road and Railroad research, Delft University of Technology

Concrete block pavements (c.b.p.) commonly consist of concrete blocks placed over a granular substructure. As a result of wheel load passages permanent strains will slowly develop in the substructure and cause rutting.
This paper is about the prediction of the permanent strain development in the substructure and the associated rutting on the basis of the results of repeated load triaxial tests and analytical models. By discussing the behaviour of three c.b.p.'s it is shown that insight into c.b.p. behaviour is obtained and that the effects of various substructure designs can be evaluated without the construction of real c.b.p.'s.

Keywords: **concrete block pavements, granular materials, stress dependent behaviour, permanent strain, rutting, theoretical modelling.**

1 Introduction

In the Netherlands approximately 35% of all road pavement area consists of small element pavements, most of them being concrete block pavements (c.b.p.'s). These c.b.p.'s consist of rectangular blocks placed over one or more layers of unbound granular material, i.e a thin bedding sand layer, an unbound granular base (not always applied) and a sand sub-base over the subgrade, Houben et al. (1988), see Figure 1. As a result of traffic passages permanent strains will slowly develop within the granular substructure of the pavement. These permanent strains lead to rutting at the surface of the pavement. If this rutting becomes too severe the pavement is considered to be failed for reasons of safety and comfort.

Given the large amount of money involved in concrete block relaying (the only solution to repair the rutting defect), c.b.p.'s should be designed such that the pavement life with respect to rutting is optimized. This is only possible if there is some knowledge on the development of permanent strains and the associated rutting.
Until now rutting predictions are made by assuming a linear relation between the development of permanent strains and resilient strains, such an approach is a poor description of reality. In this paper some results of a research project are described which was focusing on a better prediction of the development of permanent strain. This prediction is based on the behaviour of the granular

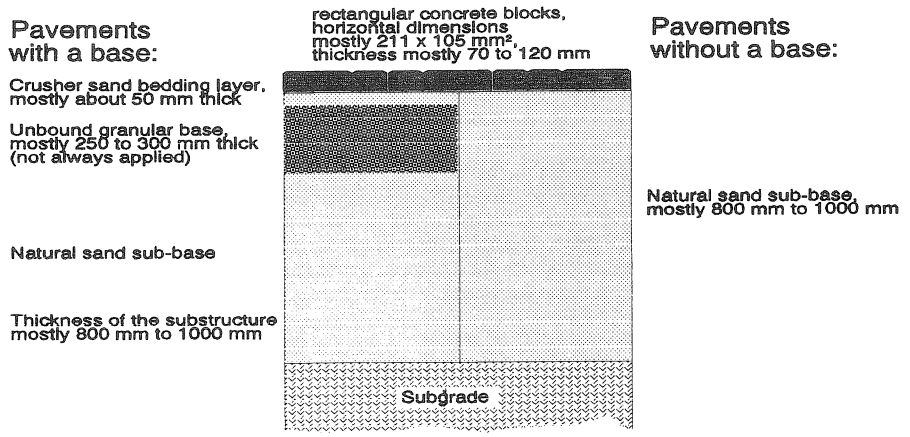

Fig. 1. Basic design of Dutch concrete block pavements.

materials used in the substructure, and on a numerical model to determine the development of permanent strains in these materials.

2 Material behaviour

2.1 *Introduction*

The material properties that are needed to predict the permanent strain development consider:

- strength,
- resilient behaviour,
- permanent strain development.

For this research eight sands (seven natural sands and one crusher sand) and four base course materials were tested in the Road and Railroad Research Laboratory of the Civil Engineering Department of the Delft University of Technology. In this paper the emphasis is laid on the behaviour of the sands. The behaviour of the base course materials is only roughly discussed.

The grain size distribution of the eight sands are presented in the Figure 2. For classification purposes the Volders and Verhoeven Sharpness (VVS) of the sands is given in Table 1. The VVS is determined by means of an outflow test and represents the grain shape by a percentage, *K*. Wester et al. (1979). The higher this percentage the sharper the grains of the sand.

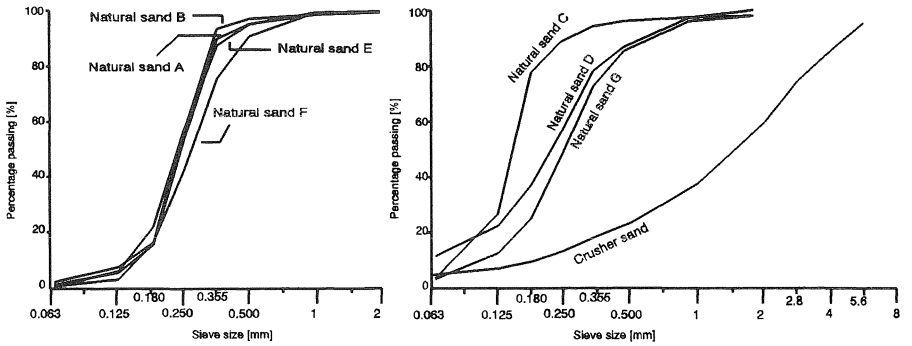

Fig. 2. Grain size distribution of the eight sands.

Table 1: Volders and Verhoeven Sharpness of the sands.

Sand	vvs [–]	Sand	vvs [–]
Natural sand A	66.52 %	Natural sand E	72.13 %
Natural sand B	72.85 %	Natural sand F	94.11 %
Natural sand C	74.29 %	Natural sand G	66.59 %
Natural sand D	72.40 %	Crusher sand	115.74 %

2.2 *Test set-up*

The earlier mentioned material properties are all determined using a triaxial test set-up, see Figure 3. For testing a sand a cylindrical sample with a height of 200 mm and a diameter of 101.6 mm is prepared. This sand sample is enclosed in a membrane and placed in a pressure cell. The sand sample is connected with the atmosphere while the pressure in the cell can be varied so that the sample can be subjected to an adjustable confining pressure σ_{conf}.
After σ_{conf} is applied by pressurising the cell, the actuator is used to subject the sample to an additional stress in the vertical direction.

2.3 *Strength of the sands*

The strength of a granular material strongly depends on σ_{conf}. The relation between the first principal stress at failure, $\sigma_{1,f}$, and σ_{conf} can be explained using the well known Mohr-Coulomb criterion. The cohesion C and angle of internal friction ϕ are in this research program determined on the basis of three static failure triaxial tests. In these tests, performed at three levels of σ_{conf}, the actuator imposes the sample to a slowly increasing vertical strain in a displacement controlled mode. The actuator force and displacement are recorded, the maximum force is used to determine the first principal stress at failure $\sigma_{1,f}$.
For example purposes the results obtained for one natural sand, natural sand E, are shown in

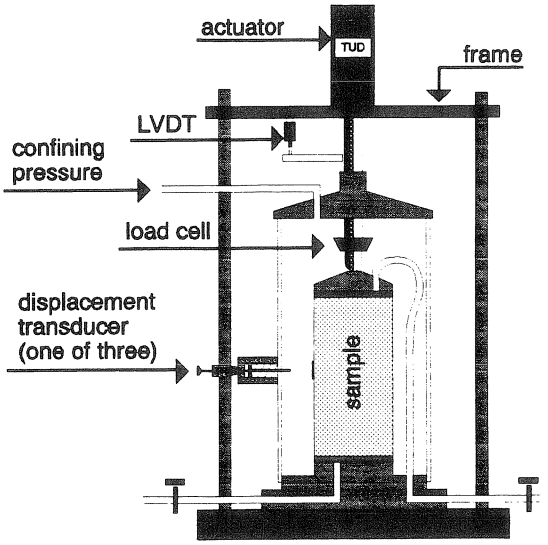

Fig. 3. The triaxial test set-up, sample size 200 × 101.6 mm².

Figure 4. As shown by this plot a very good fit between the data and the Mohr-Coulomb criterion was obtained. Similar results were obtained for the other sands, see Table 2.

Table 2. Values for C and ϕ found for the sands.

	C [kPa]	ϕ [°]		C [kPa]	ϕ [°]
Natural sand A	6.3	41.8	Natural sand E	4.1	43.9
Natural sand B	6.8	43.0	Natural sand F	5.6	48.2
Natural sand C	7.2	42.8	Natural sand G	8.0	39.7
Natural sand D	7.5	42.9	Crusher sand	8.7	50.2

2.4 *Resilient behaviour of the sands*

For the determination of the resilient behaviour of a sand a cyclic load triaxial test is performed. In these tests the stresses applied to the sample are more complex. After applying σ_{conf}, a very small static stress, σ_{stat}, is applied by the actuator. Then a halfsine-shaped cyclic stress, σ_{cycl}, is applied by the actuator, see Figure 5.

During testing σ_{cycl}, as well as the sample deformation as a result of this stress, are continuously recorded. From the measured resilient radial and axial sample deformations under the cyclic load, the resilient radial strain, ε_{rad}, and the resilient axial strain, ε_{ax}, are calculated.

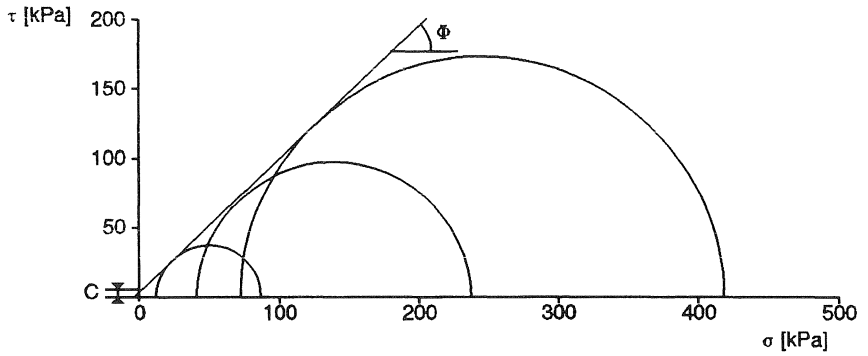

Fig. 4. Failure test results obtained for natural sand E.

The resilient modulus, *Mr*, and the Poisson's ratio, υ, can now be determined using the following equations:

$$Mr = \frac{\sigma_{cycl}}{\varepsilon_{ax}} \quad [\text{MPa}] \tag{1}$$

$$\nu = -\frac{\varepsilon_{rad}}{\varepsilon_{ax}} \quad [-] \tag{2}$$

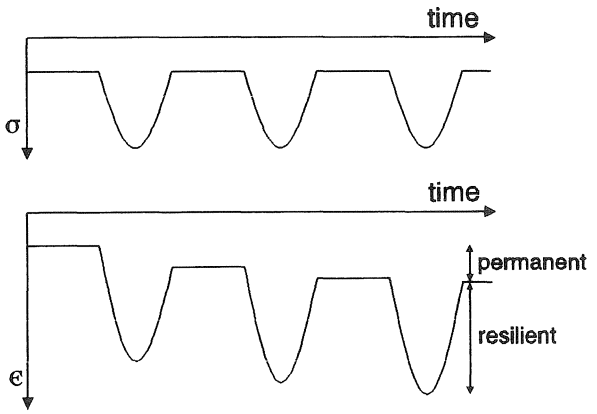

Fig. 5. Principal of the applied vertical stress and the resulting strains.

The resilient modulus defined here thus is a secant modulus.
Both *Mr* and ν appear to be stress dependent. Various models are at hand to describe this stress dependency, Sweere (1990). The most common of these resilient behaviour models describes the measured stiffness *Mr* as a function of the sum of the principal stresses θ:

$$\theta = \sigma_1 + \sigma_2 + \sigma_3 \quad [\text{kPa}] \tag{3}$$

In the described triaxial test σ_2 and σ_3 equal σ_{conf}. The first principal stress σ_1 is equal to the sum of four contirbutions, see equation 4.

$$\sigma_1 = \sigma_{conf} + \sigma_{stat} + \sigma_{dw} + \sigma_{cycl} \quad [\text{kPa}] \tag{4}$$

In this equation σ_{dw} represents the stresses as a result of dead weight.
As mentioned earlier the most common model describing the stress dependency of *Mr* is the Mr-θ model introduced by Brown and Pell (1967), see Figure 6:

$$Mr = k1\left(\frac{\theta}{\theta_0}\right)^{k2} \quad [\text{MPa}] \tag{5}$$

where: Mr = resilient modulus [MPa]
$k1$ = model parameter [MPa]
$k2$ = model parameter [–]
θ = sum of principal stresses [kPa]
θ_0 = reference stress = 1 kPa [kPa]

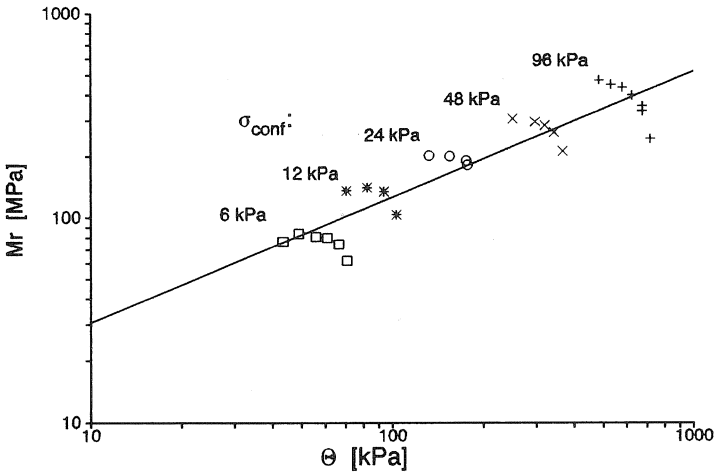

Fig. 6. The Mr-θ model combined with the Mr measuring data obtained for natural sand E.

For the other sands similar results were obtained, see Table 3.

As shown by Figure 6 and Table 3, the *Mr-θ* model describes the general trend in the data quite well. However, by distinguishing the various levels of σ_{conf} at which moduli were determined, one comes to a completely different conclusion. Per σ_{conf} level, σ_2 and σ_3 are constant. This implies that the increase of θ, at a constant level of σ_{conf}, completely depends on an increase of σ_1. For a constant

level of σ_{conf}, the data in Figure 6 clearly shows a decreasing *Mr* with an increasing θ. An increase of σ_1 thus leads to a decrease of *Mr*. The same data how-ever shows that an increase in σ_{conf}, i.e. σ_2 and σ_3, leads to an increase of *Mr*.

It is clear that the conventional *Mr*-θ model is not able to describe this behaviour since in that model an increase of both σ_3 and σ_1 lead to an increase of θ and, according to the model, to an increase of *Mr*.

Table 3. Parameters found for the *Mr*-θ model for sands.

	***k*1 [MPa]**	***k*2 [–]**	r^2
Natural sand A	18.6	0.48	0.81
Natural sand B	10.1	0.60	0.82
Natural sand C	12.6	0.55	0.84
Natural sand D	6.3	0.72	0.77
Natural sand E	7.4	0.62	0.85
Natural sand F	5.4	0.69	0.82
Natural sand G	8.2	0.67	0.79
Crusher sand	5.7	0.55	0.88

Therefore a new model was developed that is capable to describe the effects of both σ_3 and σ_1 on the development of Mr:

$$Mr = k5\left(\frac{\sigma_3}{\sigma_{3_0}}\right)^{k6}\left(1 - k7\left(\frac{\sigma_1}{\sigma_{1,f}}\right)^{k8}\right) \quad [\text{MPa}] \tag{6}$$

$$\text{with } \sigma_{1,f} = \frac{(1 + \sin\phi)\sigma_3 + 2c\cos\phi}{1 - \sin\phi} \quad [\text{kPa}] \tag{7}$$

where:
- σ_1 = first principal stress [kPa]
- $\sigma_{1,f}$ = σ_1 at failure according to Mohr-Coulomb [kPa]
- σ_3 = third principal stress or confining pressure [kPa]
- σ_{3_0} = reference stress = 1 kPa [kPa]
- *k*5 = model parameter [MPa]
- *k*6, *k*7, *k*8 = model parameters [–]
- *c* = cohesion [kPa]
- ϕ = angle of internal friction [°]

The first term in equation 6 describes the increase of *Mr* with an increase of σ_3. This dependency of *Mr* on σ_3 was earlier found by Monismith et al. (1967). The second term, describing the decrease of

Mr with an increase of σ_1, is added to the *Mr*-σ_3 model to obtain a model that describes the measured data much better than the *Mr*-θ model does, see Figure 7.

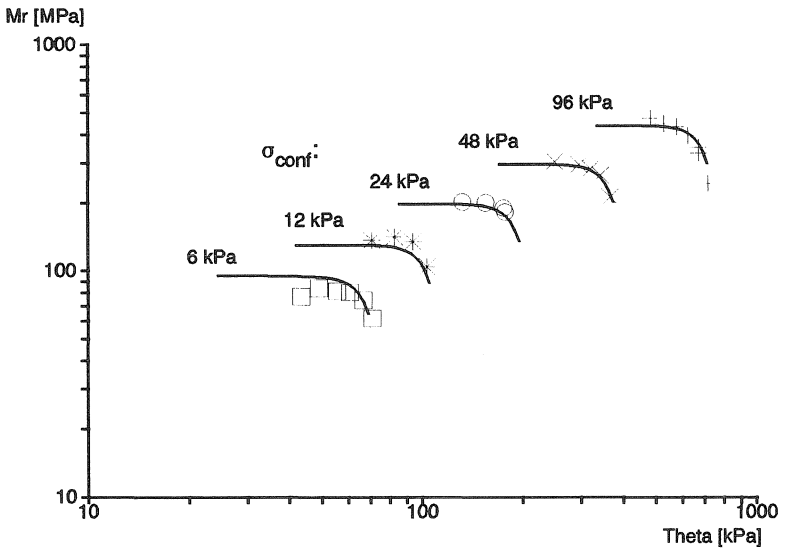

Fig. 7. The Mr-s3-s1 model and the measured Mr-values for natural sand E.

As shown by Table 4 similar results were obtained for the other sands.

Table 4. Model parameters found for the *Mr*-σ_3-σ_1 model on different sands.

	*k*5 [MPa]	*k*6 [–]	*k*7 [–]	*k*8 [–]	r^2
Natural sand A	45.95	0.52	0.36	7.05	0.96
Natural sand B	38.40	0.60	0.89	5.79	0.98
Natural sand C	44.96	0.52	0.28	5.83	0.98
Natural sand D	38.64	0.68	0.42	4.04	0.94
Natural sand E	30.42	0.59	0.47	7.68	0.98
Natural sand F	47.75	0.58	0.67	1.51	0.95
Natural sand G	34.43	0.69	0.37	4.97	0.97
Crusher sand	19.23	0.54	0.19	8.63	0.99

As mentioned earlier, the Poisson's ratio υ also shows a stress dependency. A simple equation is used to describe this ratio as a function of the $\sigma_1 / \sigma_{1,f}$-ratio, equation 8.

$$\nu = \nu 0 + \nu 1 \left(\frac{\sigma_1}{\sigma_{1,f}} \right)^{\nu 2} \quad [-] \tag{8}$$

Where: $\upsilon 0$, $\upsilon 1$, $\upsilon 2$: model parameters [–]

In Figure 8 the stress dependent Poisson's ratio and this model are shown for natural sand E, Table 5 shows that similar results are obtained for the other sands.

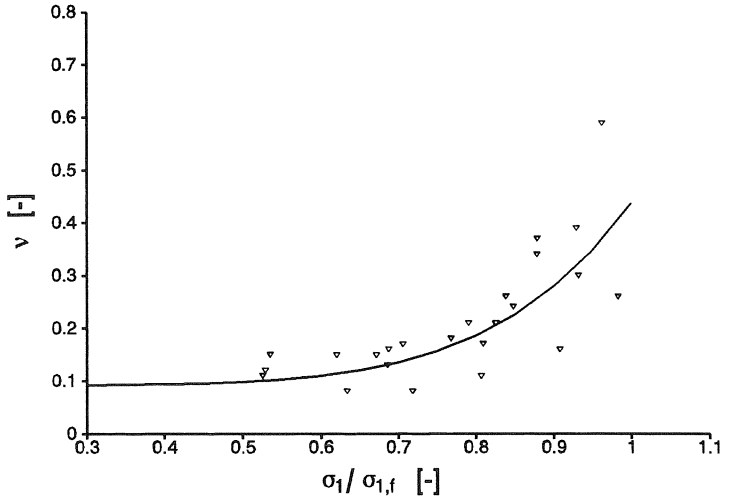

Fig. 8. The stress dependent υ as measured for natural sand E.

Table 5. Parameters found for the υ-$\sigma_1 / \sigma_{1,f}$ model for sands.

	υ 0 [–]	υ 1 [–]	υ 2 [–]	r^2
Natural sand A	0.12	0.27	6.80	0.87
Natural sand B	0.17	0.58	4.23	0.91
Natural sand C	0.15	0.23	4.61	0.89
Natural sand D	0.04	0.40	1.48	0.59
Natural sand E	0.09	0.35	5.82	0.66
Natural sand F	0.13	0.45	3.95	0.30
Natural sand G	0.10	0.31	2.39	0.69
Crusher sand	0.11	0.54	1.72	0.97

2.5 *Permanent strain development in the sands*

The development of permanent strain in the sands is measured by applying up to one million load cycles in a cyclic load triaxial test.

The permanent strain triaxial tests were all performed at a confining stress, σ_{conf}, of 12 kPa. During testing the actuator loaded the sample with a small static stress, σ_{stat}, and a much larger cyclic stress, σ_{cycl}. The cyclic stress was again halfsine-shaped.

The permanent strain triaxial tests again showed stress dependent behaviour, see Figure 9. With an increase of $\sigma_1 / \sigma_{1,f}$ a more serious permanent strain development was observed. This behaviour is described by the equations 9 to 13.

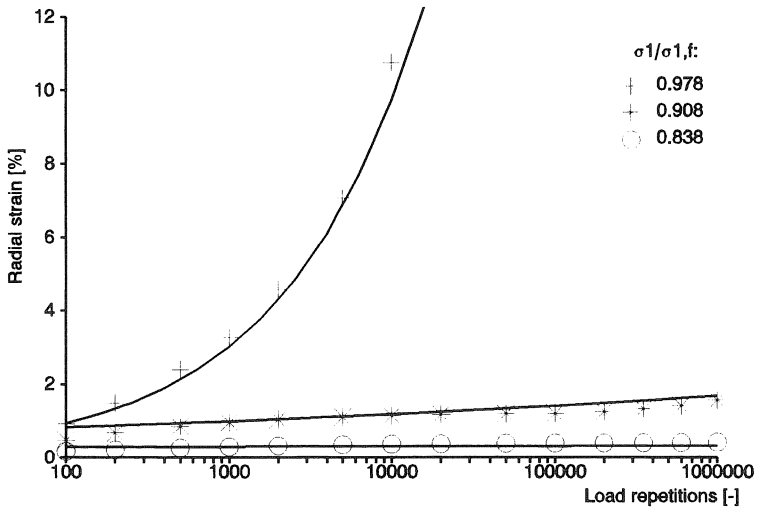

Fig. 9. Permanent radial strain development as measured for the Zaanweg sand.

Equation 9 is commonly used to describe creep curves measured for asphalt mixes, for instance Francken et al. (1987). Equations 10 to 13 are used to describe the stress dependency in the measured permanent strain development.

$$\varepsilon_{perm} = A\left(\frac{N}{1000}\right)^{B} + C\left(\exp\left(D\frac{N}{1000}\right) - 1\right) \quad [-] \tag{9}$$

$$A = a1\left(\frac{\sigma_1}{\sigma_{1,f}}\right)^{a2} \quad [-], \qquad B = b1\left(\frac{\sigma_1}{\sigma_{1,f}}\right)^{b2} \quad [-], \tag{10), (11}$$

$$C = c1\left(\frac{\sigma_1}{\sigma_{1,f}}\right)^{c2} \quad [-] \text{ and} \qquad D = d1\left(\frac{\sigma_1}{\sigma_{1,f}}\right)^{d2} \quad [-] \tag{12), (13}$$

Where: ε_{perm} = permanent strain [–]
N = number of applied load cycles [–]
$a1,a2,b1,b2$ = model parameters [–]
$c1,c2,d1,d2$ = model parameters ($c1,c2,d1,d2$ equal 0 in case of sands) [–]

The equations given above apply for both the radial and axial permanent strain, see Figure 9 and 10.

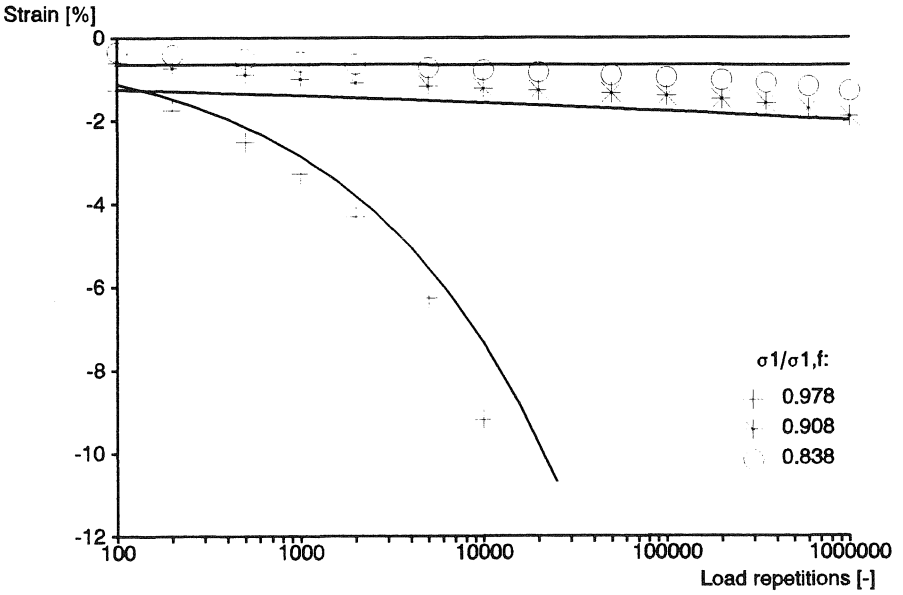

Fig. 10. Development of permanent axial strain in natural sand E.

Similar results are obtained for the other sands, see Table 6 and 7.

Table 6. Model parameters found for the development of permanent axial strain in various sands.

	$a1\%$ [–]	$a2$ [–]	$b1$ [–]	$b2$ [–]	r^2
Natural sand A	–5.01	16.40	0.30	20.07	0.85
Natural sand B	–2.72	6.64	0.27	6.05	0.99
Natural sand C	–2.54	5.26	0.07	0.00	0.86
Natural sand D	–4.97	4.96	0.31	13.27	0.82
Natural sand E	–3.53	9.59	0.76	27.80	0.80
Natural sand F	–5.19	5.93	0.14	1.13	0.88
Natural sand G	–5.46	6.61	0.29	6.06	0.95
Crusher sand	–2.76	2.69	0.18	0.50	0.70

Table 7. Model parameters found for the development of permanent radial strain in various sands.

	$a1\%$ [–]	$a2$ [–]	$b1$ [–]	$b2$ [–]	r^2
Natural sand A	5.98	22.63	0.34	20.93	0.70
Natural sand B	3.13	9.16	0.32	8.67	0.98
Natural sand C	2.03	6.09	0.09	2.49	0.83
Natural sand D	5.42	7.75	0.40	29.47	0.91
Natural sand E	4.20	14.89	0.90	25.44	0.95
Natural sand F	6.82	8.29	0.16	2.38	0.91
Natural sand G	6.50	9.12	0.51	10.04	0.95
Crusher sand	3.23	4.88	0.18	0.34	0.705

2.6 *Base course materials*

In this research also four base course materials (crushed concrete/masonry mixes) were considered. Using a much larger triaxial test set-up, the same tests as performed on the sands were also performed on these base materials. In this paper the laboratory results obtained for these base materials are not given, they are discussed elsewhere by van Niekerk et al. (1995). The most significant differences between the observed behaviour of sands and base materials are shortly discussed hereafter.

Strength:

The base materials can resist much larger σ_1 than sands can at the same σ_{conf}-level. Especially the cohesion of the base materials is much larger than the cohesion of the sands.

Resilient behaviour:

The base materials were not tested up to a $\sigma_1 / \sigma_{1,f}$-ratio close to 1 for two reasons. First of all because such high ratios do not occur within the base course of a concrete block pavement structure and secondly because base materials show a large permanent strain development at these high ratios.

Because the tests were done at limited $\sigma_1 / \sigma_{1,f}$-ratios a decrease of Mr with increasing σ_1 was not measured. As a result the Mr-θ model had to be used to fit with the measured data.

The base materials have a much larger ν than the sands. At small stress ratios, the measured ν is about 0.4, at larger stress ratios ν-values up to about 1 were measured.

Permanent strain development:

The base course materials show a significant permanent strain development at $\sigma_1 / \sigma_{1,f}$-ratios larger than 0.4 to 0.5. Given the high strength of the base materials the absolute stresses at these ratios are however higher than the stresses in a sand at a $\sigma_1 / \sigma_{1,f}$-ratio close to 1.

In two out of four course base materials the values of $c1$, $c2$, $d1$ and $d2$, equations 9 to 13, were not equal to zero as was the case for the sands. These materials thus show an increase in the rate of permanent strain development when a sufficient number of load repetitions is applied.

3 Resilient behaviour of concrete block pavement structures

3.1 *Introduction*

For the analysis of the resilient behaviour of concrete block pavements the stress dependent resilient behaviour of the unbound granular materials, applied in such pavements, clearly has to be taken into account. For this reason an axial symmetric finite element model was developed.
In this chapter the most important characteristics of this model are discussed. Hereafter the calculation results obtained for three concrete block pavements are discussed.

3.2 *Geometry of the pavement model*

The geometry of the axial symmetric finite element model of the concrete block pavement structure is straight forward, see Figure 11. The elements used are simple four node elements with eight degrees of freedom. The size of these elements grows with both the radius and the depth. The smallest elements are found in the centre of the model directly under the concrete blocks and have a height of 25 mm and a width of 32 mm.

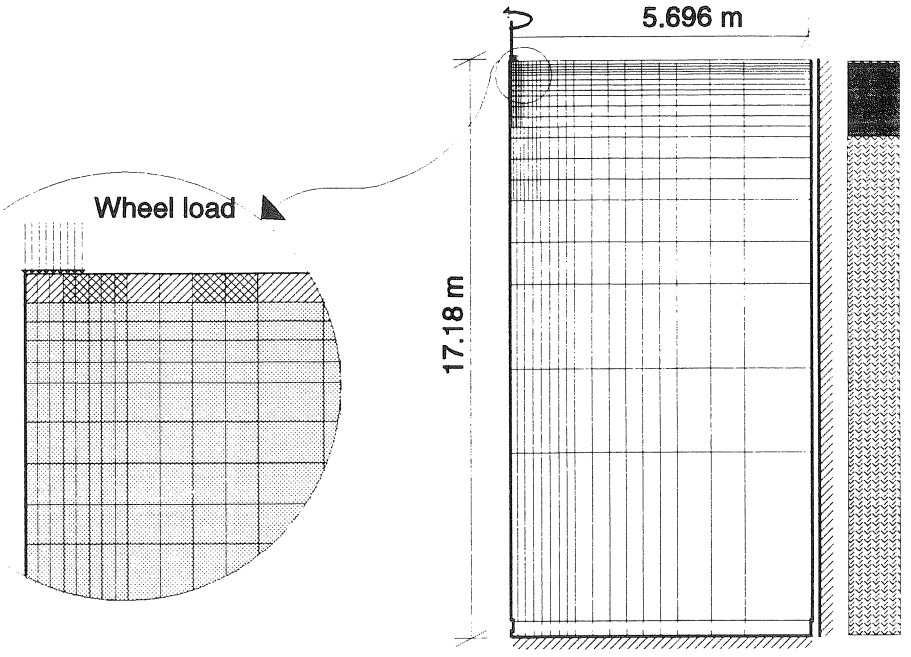

Fig. 11. Basic geometry of the Finite Element Model used for the resilient analysis of concrete block pavements.

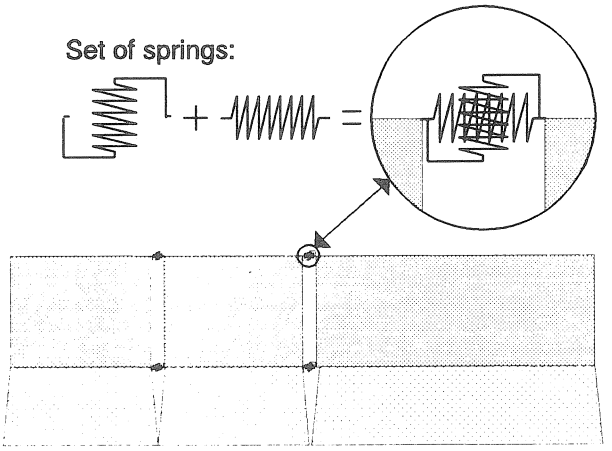

Fig. 12. Representation of the concrete block layer.

In developing this model special attention is given to the representation of the concrete block layer, see Figure 12. The block pattern that is most commonly used in the Netherlands, herringbone bond, does certainly not answer to axial symmetry, see Figure 13. Such a pattern really asks for 3-D modelling, Huurman et al. (1992). An axial symmetric model however has two major advantages over a 3-D model: it shows a very simple geometry and it requires far less degrees of freedom than a 3-D model.

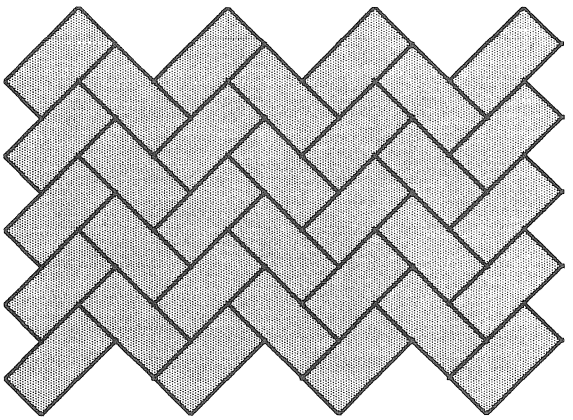

Fig. 13. Blocks in herringbone bond.

In order to overcome largely the disadvantages of an axial symmetric representation of the block layer, the elements that are used in the representation of the blocks have been taken their ability to build up normal stresses in the θ-direction, $\sigma_{\theta\theta} = 0$. As a result the blocks now have two additional types of stress-free movements, see Figure 14.

Through this modification the modelled concrete block layer no longer shows self confining properties. Furthermore the modelled blocks are able to rotate and thus introduce joint normal forces that act to expand the block layer. The behaviour of the modelled block layer is now similar to a real concrete block layer, Huurman (1994a).

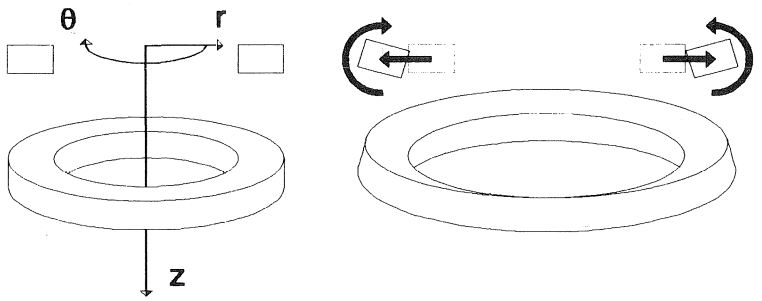

Fig. 14. The elements used in the representation of the concrete blocks are given two additional types of stress-free movements.

The joints between the blocks are represented by sets of normal and shear springs, Figure 12. These springs are both linear elastic and active in case of joint compression, the stiffness of the joint normal springs equals 550 N/mm per mm modelled joint for the shear springs the stiffness equals 50 N/mm/mm. In case of joint expansion (tensile normal joint forces) both springs are inactive. The stiffnesses of the joint springs are based on linear elastic back calculations of the deflection bowls measured (falling weight deflection measurements) on the pavements from which the tested sands and base materials were taken.

3.3 *Calculation procedure*

In this paper three pavement analyses are discussed. In all cases the pavement structure has a height of 1080 mm. The first layer has a thickness of 80 mm and represents the concrete block layer (E = 40,000 MPa, ν = 0.2). Pavement structure number 1 only has a 1000 mm thick sand sub-base (stress dependent resilient behaviour of natural sand E).
The other two pavements have an unbound granular base. These pavements both have a 50 mm thick bedding sand layer (stress dependent resilient behaviour of crusher sand). Below this bedding layer the base layer is situated (stress dependent Mr of a base course material, ν =0.49). In case of pavement structure number 2 this base has a thickness of 200 mm, while structure number 3 has a 300 mm thick base. These base layers are placed over a natural sand E sub-base layer with a thickness of 750 and 650 mm respectively.
In all cases the pavement structure is placed over the subgrade (E = 60 MPa, ν = 0.45). The three pavement structures are all loaded by a 50 kN wheel load with a circular contact area with a radius of 150 mm.

Given the stress dependent behaviour of the materials used in the substructure, the finite element program first calculates the stresses throughout the substructure on the basis of estimated

stiffnesses. The next calculation is however based on the stiffnesses that follow from these stresses in combination with the stress dependent properties of the various materials that are present in the modelled pavement structure. This iterative process is repeated until the difference between the stiffnesses (and Poisson's ratios) on which the last computed stresses are based and the stiffnesses that follow from these stresses is less than 5% in all elements.

3.4 *Calculation results*

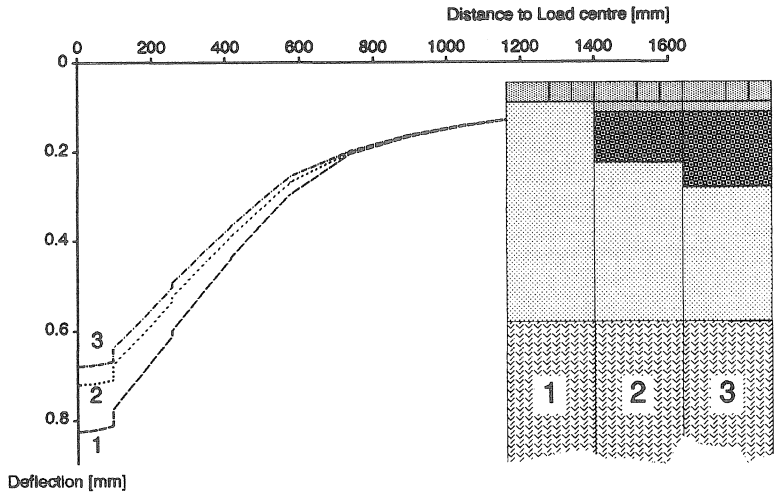

Fig. 15 Deflection bowls as calculated for the three concrete block pavements.

One of the few things that can be measured in/on a real concrete block pavement is the deflection under a (simulated) wheel load. Figure 15 shows the deflection bowls as calculated for the three pavements that are discussed here. This figure clearly shows the discontinuous character of the concrete block layer. The effects of the discussed modification of the elements used in the representation of the concrete blocks are clearly reflected, i.e. block rotation and thus block translation in *r*-direction.

As discussed earlier the goal of this research is to explain and understand the development of permanent strain in a block pavement. For this purpose the $\sigma_1 / \sigma_{1,l}$-ratio is most important, Figure 16 shows this ratio as determined for locations under the centre of the wheel load.

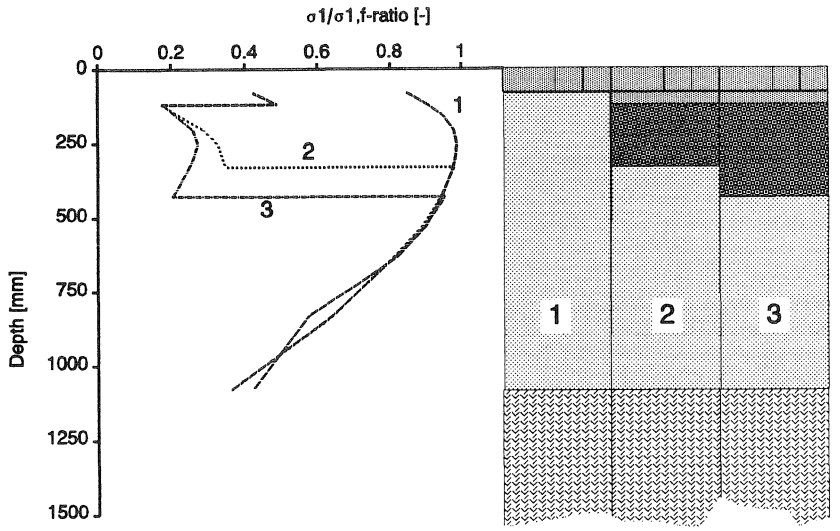

Fig. 16 The $\sigma_1/\sigma_{1,f}$-ratio over the height of the concrete block pavement structure in the centre of the model.

Figure 16 shows that the sub-base sand is subjected to large stress-ratios. In case of a pavement without a base layer the $\sigma_1 / \sigma_{1,f}$-ratio is very close to 1 at a depth of about 250 mm. At this depth the base layers are situated. In these base layers much smaller $\sigma_1 / \sigma_{1,f}$-ratios are computed (<0.4).
As shown by Figure 16 the bedding sand above the base layers also shows relatively small $\sigma_1 / \sigma_{1,f}$-ratios when compared to the situation in the pavement without a base.
Of course the $\sigma_1 / \sigma_{1,f}$-ratio is known throughout the substructure of the block pavement. In the next chapter it is explained how this computed $\sigma_1 / \sigma_{1,f}$-ratio is used to determine the expected permanent strain development in the substructure of the concrete block pavement.

4 Permanent strain development

4.1 *Calculation procedure*

The next step in the computation of the expected permanent strain development in the substructure of a concrete block pavement is explained hereafter.
It is clear that the results of the resilient analysis amongst others give insight into the $\sigma_1 / \sigma_{1,f}$-ratio throughout the substructure. Also the direction of the principal stresses is known throughout the substructure. The combination of this information with the stress dependent permanent deformation behaviour of the various materials, Figures 9 and 10 and Tables 6 and 7, makes it possible to compute the expected permanent horizontal and vertical strain development throughout the substructure of the pavement. Without further action this permanent strain development would however refer to the non-realistic situation of traffic showing absolutely no lateral wander.

Buiter et al. (1989) showed that the transversal distribution of heavy vehicles as a result of lateral wander can be described by a standard normal distribution as schematically shown in Figure 17.

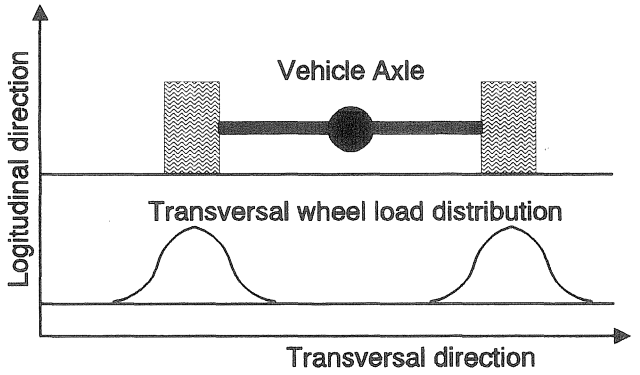

Fig. 17. Schematized lateral distribution of wheel loads in real traffic.

To take into account the effects of lateral wander, first the vertical permanent strains due to wheel loads in the centre of the wheel track are summed-up over the height of the substructure and so give the permanent vertical displacement of the surface of the pavement. This displacement of-course depends on the number of load repetitions, N. In this way the development of permanent surface displacement as a function of N can be computed for any distance from the load centre. The standard normal distribution of the wheel loads is then accounted for by shifting the calculated development of permanent surface displacement according to the standard normal distribution of wheel loads, Mooren et al. (1994). In this calculation it is assumed that the permanent surface displacement introduced by a wheel load depends on the existing permanent surface displacement, caused by previous wheel load passages. In other words, it is assumed that the damage is important and not the way this damage is formed.

4.2 *Calculation results*

In Figure 18 the development of permanent vertical strain in the centre of the rut is given for the concrete block pavement without a base (pavement 1, Figure 15). The standard deviation of lateral wander, σlw, in this computation was 100 mm, which is extremely small for normal road traffic. The figure shows that the largest vertical permanent strains develop at a depth of somewhat more than 250 mm. The rut depth reaches 15 mm, which is mostly considered as failure, after less than 5,500 load repetitions. The maximum permanent vertical strain at that moment is almost 5%.

When σlw is doubled the permanent strain development is reduced, and as a result the pavement will now last longer. A 15 mm rut depth is now reached after about 10,000 load repetitions, see Figure 19. The maximum permanent vertical strain, at this moment is somewhat larger than 5%.

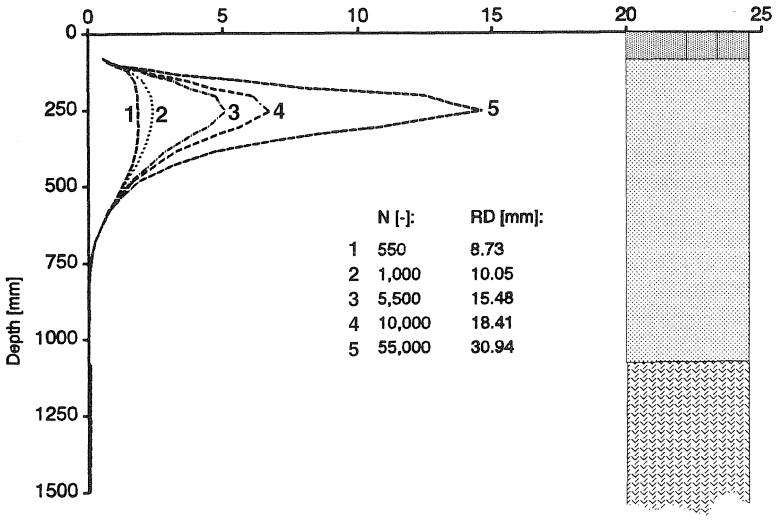

Fig. 18 Permanent vertical strain development in the rut centre for the pavement structure without a base, σlw = 100 mm.

By applying a base layer the resistance of the pavement against permanent deformation increases. In case of the thin 200 mm base (pavement 2, Figure 15), larger permanent vertical strains develop at the bottom of the base. This process starts after about 100,000 load cycles and will eventually lead to failure of the pavement, see Figure 20. A rut depth of 15 mm is now reached after about 600,000 load repetitions.

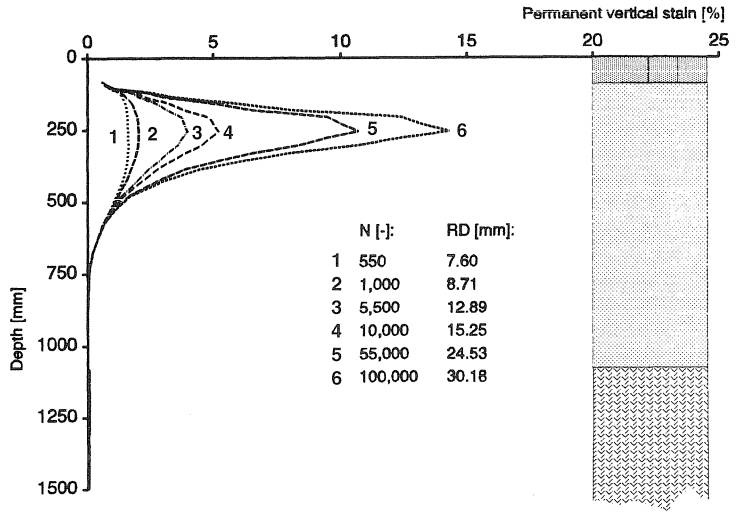

Fig. 19. Permanent vertical strain development in the rut centre for the pavement structure without a base, σlw = 200 mm.

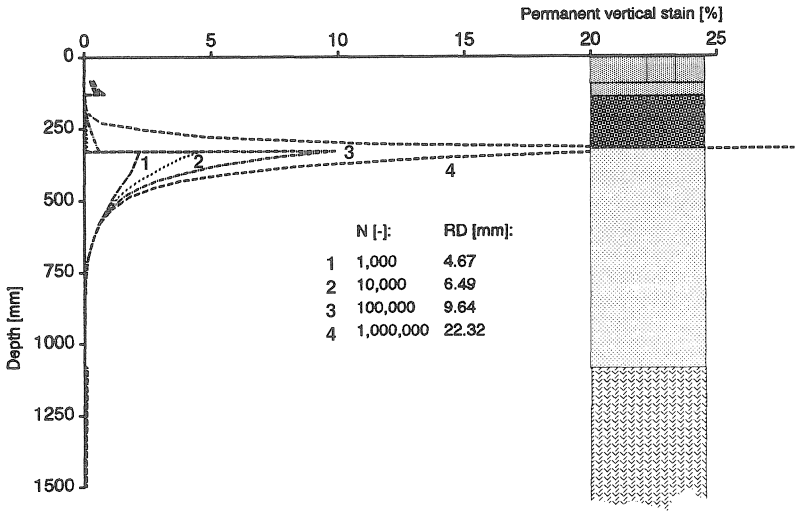

Fig. 20. Permanent vertical strain development in the rut centre for the pavement structure with a 200 mm base, σlw = 200 mm.

By increasing the thickness of the base layer to 300 mm (pavement 3, Figure 15), premature failure in this layer is prevented. In this case the largest permanent strains will develop at the top of the sand sub-base layer, see Figure 21 (in Figure 21 the scale of strain is much smaller than in the Figures 18, 19 and 20).

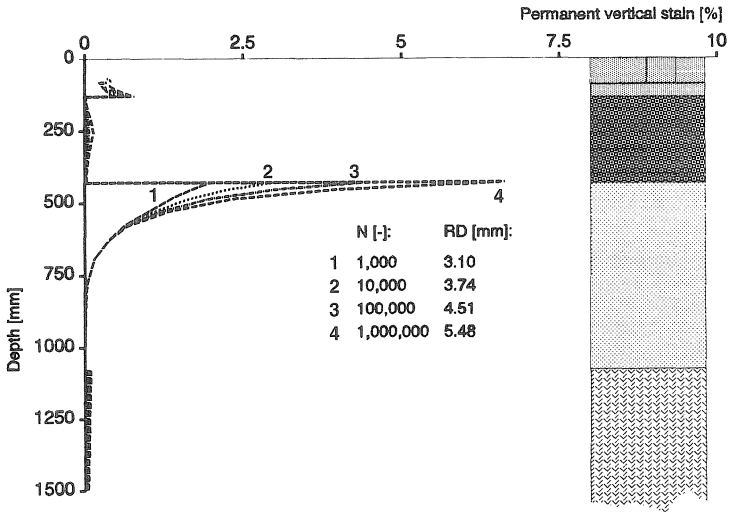

Fig. 21. Permanent vertical strain development in the rut centre for the pavement structure with a 300 mm base, σlw = 200 mm.

The block pavement with a 300 mm thick base layer shows a very strong resistance against permanent strain. After 1,000,000 load repetitions it only shows a rut depth of about 5.5 mm. More than half this rut depth is formed during the first 1,000 load repetitions which implies that the pavement structure is very stable.

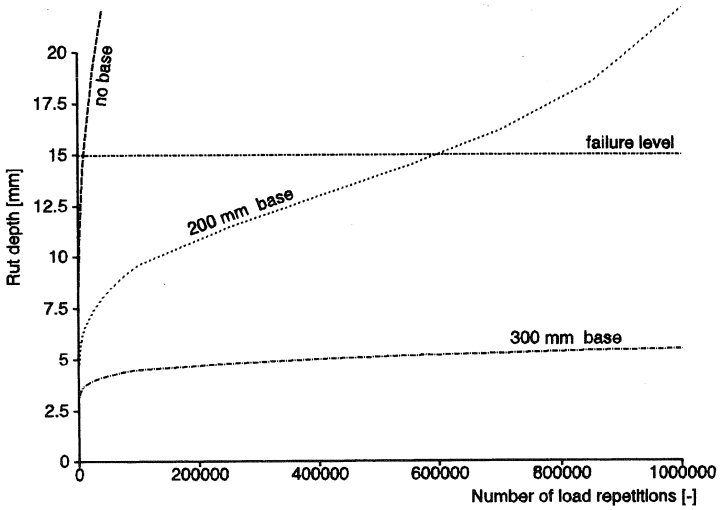

Fig. 22. Rut development in three concrete block pavement structures.

In Figure 22 the rut development for each of the three pavement structures is presented. When no base layer is applied the pavement keeps accumulating damage rapidly until it reaches failure. When a 200 mm base layer is applied the pavement will rapidly accumulate damage until it shows a rut depth of about 10 mm. After reaching this initial rut depth further accumulation of damage takes place at a much slower rate. As a result of the large initial rut depth drivers will experience a low quality concrete block pavement during the main part of the pavements life.
Figure 22 shows that applying a thick base does not only extent the life of a pavement, but also the quality of this pavement during its life. In case of the pavement structure with a 300 mm thick base the initial rut depth is about 4 mm. During the largest part of the life of this particular pavement the accumulated damage only shows minor proportions, drivers thus experience a high quality concrete block pavement.

It is obvious that by varying layer thicknesses, layer materials, wheel load magnitudes, wheel load contact areas, the standard deviation of lateral wander, and the stiffness of the subgrade a more general insight into the behaviour of concrete block pavements is obtained.

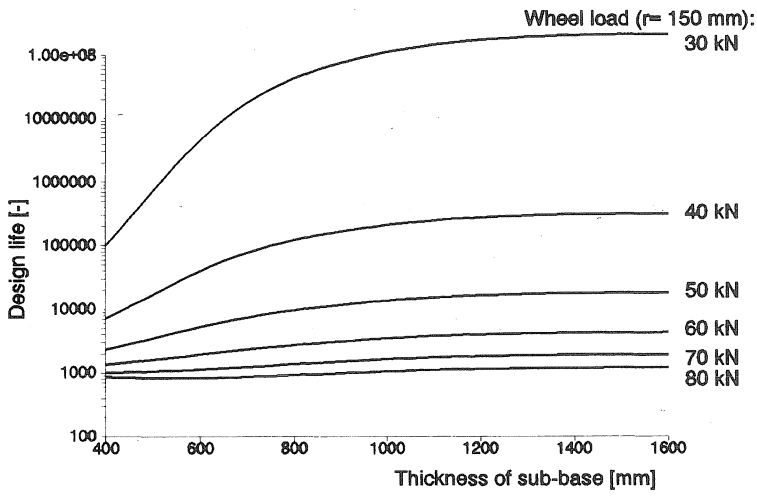

Fig. 23. Design life for block pavements with a natural sand E sub-base only (allowable rut depth 15 mm).

Figure 23 gives an example of this insight. It shows the effects of the wheel load and the thickness of the sand sub-base on the expected life of a concrete block pavement. The figure refers to a subgrade stiffness of 60 MPa and a standard deviation of lateral wander of 200 mm, again on the basis of the properties of natural sand E.
The figure shows that the computed design life of a pavement decreases if the magnitude of the load increases. It furthermore shows that concrete block pavements with only a natural sand E sub-base have a limited design life. Increasing the thickness of the sub-base has a strong positive effect on this life if only minor wheel loads up to about 30 or 40 kN are expected. For larger wheel loads the effects of increasing the thickness of the sub-base are much smaller.

5 Discussion

The research described in this paper contributes to the knowledge of concrete block pavement behaviour. Until now most of this knowledge is based on observations of real in-service pavements.
On the basis of the work presented in this paper it is possible to estimate the effects of new substructure designs on the behaviour of a concrete block pavement using the results of repeated load triaxial tests and analytical models.
As shown, this research gives insight into the effects of various wheel load magnitudes on the rut development in a pavement. Within this research also vehicle simulation is involved. Such simulations of course result in dynamic axle loads which are not constant, Huurman (1994b). Knowing the effects of various wheel load magnitudes on rut development, it is possible to determine the rut development as a result of the dynamic wheel loads.
Like the dynamic wheel loads, this rut depth is of course not constant in the longitudinal direction

of the road and will thus have effects on the longitudinal profile. A second (simulated) vehicle will thus travel a slightly different longitudinal profile then the first vehicle. By repeating such simulations insight into the effects of vehicles on the development of both longitudinal and transversal unevenness is obtained. Validation of the presented work on the basis of measured longitudinal and cross profiles will now be possible.

6 Acknowledgements

The following institutes are gratefully acknowledged for financially supporting this research into Concrete Block Pavement behaviour:

STW	Netherlands Technology Foundation,
VNC	Dutch Cement Association,
Febelcem	Belgium Cement Association,
Centre ROW	Centre for Research and Contract Standardization in Civil and Traffic Engineering – The Netherlands,
Fabes	Dutch Association of Concrete Paving Block Manufacturers,
NVWB	Dutch Association of Road Contractors and the Municipal Works Rotterdam.

7 References

BROWN, S.F. and PELL, P.S. (1967), An experimental investigation of the stresses, strains and deflections in a layered pavement structure subjected to dynamic loads, In *Proceedings Second International Conference Structural Design of Asphalt Pavements*, Ann Arbor, USA, pp. 487-504.

BUITER, R., CORTENRAAD, W.M.H., ECK, A.C. VAN and RIJ, H. VAN (1989), Effects of Transversal Distribution of Heavy Vehicles on Thickness Design of Full-Depth Asphalt Pavements, In *Transportation Research Record TRR 1227*, Transportation Research Board TRB, Washington, DC, USA, pp. 66-74.

FRANCKEN, L. and CLAUWAERT, C. (1987), Characterization and structural Assessment of bound materials for flexible road structures, In *Proceedings Sixth International Conference Structural Design of Asphalt Pavements*, Ann Arbor, USA, pp. 130-144.

HOUBEN, L.J.M., et al. (Working Group D3 'Design of small element pavements' of Centre R.O.W.) (1988), The Dutch design method for concrete block road pavements, In *Proceedings Third International Conference on Concrete Block Paving*, Rome, pp. 156-169.

HUURMAN, M., HOUBEN, L.J.M. and KOK, A.W.M. (1992), Development of a Three-Dimensional Finite Element Model for Concrete Block Pavements, In *Proceedings Fourth International Conference on Concrete Block Paving*, Auckland, New Zealand, Volume 1, pp. 89-98.

HUURMAN, M. (1994a), Development of the Non-linear Finite Element Program Nolip for Concrete Block Pavements, In *Proceedings Second International Workshop on Concrete Block Paving*, Oslo, Norway, pp. 157-166.

HUURMAN, M. (1994b), Longitudinal Unevenness and Dynamic Axle loadings on Concrete Block

Pavements, In *Proceedings Second International Workshop on Concrete Block Paving*, Oslo, Norway, pp. 203-215.

MONISMITH, C.L., SEED, H.B., MITRY, F.G. and CHAN, C.K., Prediction of pavement deflections from laboratory tests, In *Proceedings Second International Conference Structural Design of Asphalt Pavements*, Ann Arbor, USA, pp. 109-140.

MOOREN, F.F.G. and HUURMAN, M. (1994), Rut Development in Concrete Block Pavements, Laboratory for Road and Railroad Research, Delft University of Technology, Delft, report 7-94-200-15.

NIEKERK, A.A. VAN and HUURMAN, M. (1995), Establishing Complex Behaviour of Unbound Road Building Materials from Simple Material Testing, Laboratory for Road and Railroad Research, Delft University of Technology, Delft, report 7-95-200-16.

SWEERE, G.T.H. (1990), Unbound Granular Bases for Roads (PhD dissertation), Delft University of Technology, Delft, The Netherlands.

WESTER, K. et al. (Working Group F4 'sub base' of Centre R.O.W.) (1979), Various Properties of Natural Sands for Netherlands Highway Engineering, Arnhem, The Netherlands.